

NACA RM L56C16

9837

~~CONFIDENTIAL~~

Copy 196
RM L56C16



Ref # 14478
MAY 1956

0144202



TECH LIBRARY KAFB, NM

RESEARCH MEMORANDUM

EFFECT OF WING CAMBER AND TWIST AT MACH NUMBERS FROM 1.4
TO 2.1 ON THE LIFT, DRAG, AND LONGITUDINAL STABILITY
OF A ROCKET-POWERED MODEL HAVING A 52.5°
SWEPTBACK WING OF ASPECT RATIO 3

AND INLINE TAIL SURFACES

By Warren Gillespie, Jr.

Langley Aeronautical Laboratory
Langley Field, Va.

HADC
TECHNICAL LIBRARY
AFL-2811

~~CONFIDENTIAL~~
This material contains information affecting the National Defense of the United States within the meaning of the espionage laws, Title 18, U.S.C., Sec. 793 and 794, and the transmission or the revelation of its contents in any manner to an unauthorized person is prohibited by law.

NATIONAL ADVISORY COMMITTEE
FOR AERONAUTICS

WASHINGTON

May 7, 1956

~~CONFIDENTIAL~~



0144202

NATIONAL ADVISORY COMMITTEE FOR AERONAUTICS

RESEARCH MEMORANDUM

EFFECT OF WING CAMBER AND TWIST AT MACH NUMBERS FROM 1.4

TO 2.1 ON THE LIFT, DRAG, AND LONGITUDINAL STABILITY

OF A ROCKET-POWERED MODEL HAVING A 52.5°

SWEEPBACK WING OF ASPECT RATIO 3

AND INLINE TAIL SURFACES

By Warren Gillespie, Jr.

SUMMARY

A free-flight investigation has been made to determine the effect of wing camber and twist at Mach numbers from 1.4 to 2.1 on the lift, drag, and longitudinal stability of a configuration having a 52.5° sweptback wing of aspect ratio 3, and inline tail surfaces. The wing was cambered and twisted to have low drag at a wing lift coefficient of 0.3 and at a Mach number of 1.46. The method reported in NACA Report 1226 was used to determine the wing warp. The model was aerodynamically pulsed in pitch throughout the flight of the model alone. Drag polars, normal force, pitching moment, static longitudinal stability, and wash effects at the horizontal tail were obtained. Comparisons are made with data from a similar model that had a flat (untwisted and uncambered) wing.

The maximum wing lift coefficient attained during the flight test was generally somewhat less than the wing design lift coefficient of 0.3. The warped wing working in conjunction with a relatively large unswept horizontal tail gave approximately the same model drag as the flat wing at the highest test lift coefficients and at the same Mach number. The wing twist and camber increased the minimum drag coefficient by the amounts 0.002 at the wing design Mach number of 1.46, and 0.003 at a Mach number of 2.1. The normal-force-curve slope was increased approximately 0.004 and the static margin approximately 5 percent of the wing mean aerodynamic chord.

~~CONFIDENTIAL~~~~17 56-842~~

INTRODUCTION

The effectiveness of two methods of wing warp in reducing drag due to lift at supersonic Mach numbers has been experimentally demonstrated for a few tailless wing-body configurations (refs. 1, 2, and 3). The conical-camber method investigated in references 1 and 2 is the simpler method but is restricted in the sense that the principal effort is directed toward minimizing the induced (vortex) drag component of the drag due to lift by maintaining an approximately elliptical spanwise loading. An effective leading-edge suction force of some undetermined extent is developed by the camber and twist whereas a special condition is imposed to reduce drag that might arise from excessive twist at the root-chord region of the wing. The sum of the vortex and wave drag is therefore not necessarily minimized by this method but may have a relatively low value. The compound warp method first reported in reference 4 and extended later in references 3 and 5 is more flexible in the conditions that can be imposed on the wing. This method is based on an assumed variation of the lifting-pressure coefficient over the wing. The use of reference 5 in conjunction with reference 4 permits the direct determination of the surface shape and ordinates for least drag due to lift corresponding to the assumed variation of the lifting pressure coefficient. The assumed variation of lifting-pressure coefficients itself may not be an optimum. Thus neither method (conical camber or compound warp) necessarily gives an absolute minimum to the sum of the vortex and wave drag. Both methods are presently applicable only to wing plan forms swept within the Mach cone originating from the wing apex. Neither method takes into account wing-body interference which should be an important consideration for the low-aspect-ratio wings proposed for flight at supersonic speeds.

The purpose of the present brief investigation is to determine experimentally whether any benefits can be realized by employing the compound warp method at a design Mach number of 1.46 and a wing lift coefficient of 0.3 on a 52.5° sweptback-wing configuration having an inline tail. At this Mach number and wing lift coefficient reference 4 was used together with arbitrary spanwise and chordwise loading distributions to determine the wing twist and camber. The model was flight tested at Mach numbers from 1.4 to 2.1 at the Langley Pilotless Aircraft Research Station at Wallops Island, Va. The horizontal tail was aerodynamically pulsed continuously between stop settings of $\pm 2.0^\circ$. The basic aerodynamic parameters in pitch were determined from the response of the model to the approximate square-wave tail motion.

SYMBOLS

C_N	normal-force coefficient, $\frac{a_n}{g} \frac{W}{S}$
C_C	chord-force coefficient, $\frac{-a_l}{g} \frac{W}{S}$
C_L	lift coefficient, $C_N \cos \alpha - C_C \sin \alpha$
C_D	drag coefficient, $C_C \cos \alpha + C_N \sin \alpha$
C_m	pitching-moment coefficient about $0.55\bar{c}$, $\frac{I_y \ddot{\theta}}{qS\bar{c}}$
$\frac{C_1}{C_L}, \frac{C_2}{C_L}, \frac{C_3}{C_L}, \frac{C_4}{C_L}$	wing-warp-design loading constants
c_l	local lift coefficient based on local chord, $\frac{\text{Lift per unit span}}{qc}$
c_l'	local lift coefficient based on local span, $\frac{\text{Lift per unit chord}}{qb'}$
P	lifting-pressure coefficient, $\Delta p/q$
a_n	normal acceleration, ft/sec^2
a_l	longitudinal acceleration, ft/sec^2
g	acceleration due to gravity, 32.2 ft/sec^2
q	dynamic pressure, lb/sq ft
V	velocity, ft/sec
M	Mach number
m	cotangent of sweepback angle of wing leading edge, 0.656

m_1	cotangent of sweepback angle of wing trailing edge, 1.571
$k \equiv \frac{m}{m_1} = 0.417$	
R	Reynolds number, where reference length is 1 ft
λ	taper ratio, $\frac{\text{Tip chord}}{\text{Root chord at center line}}$, 0.2
Λ	angle of sweep of quarter-chord line, deg
W	weight of model, lb
$\ddot{\theta}$	angular acceleration in pitch, radians/sec ²
S	total wing area to body center line, 4.00 sq ft
b	total wing span, 3.46 ft
b'	portion of local wing span covered by wing, ft
\bar{c}	wing mean aerodynamic chord, 1.32 ft
c	local wing chord, ft
c_r	wing root chord, ft
α	angle of attack, deg
β	angle of sideslip, deg
δ	horizontal tail deflection from body center line, deg
I_y	model moment of inertia in pitch about center of gravity, slug-ft ²
Δp	difference in static pressure on upper and lower surfaces, lb/sq ft
$\sigma \equiv y/s$	
s	semispan, b/2
x, y, z	rectangular coordinates with origin at wing apex
x'	distance in x-direction from leading edge of local chord

MODEL

A drawing of the cambered wing model of the present test is shown in figure 1 and photographs of the model are presented in figure 2. Geometric and mass characteristics of the model are listed in tables I and II. The model was identical to the model of reference 6 except for a more rearward location of the total-pressure tube on the top of the body, the absence of a fin-mounted flow indicator and a tail-mounted total-pressure tube, and the warp of the wing. The ratio of the maximum diameter of the body to the wing span was 0.168. A 52.5° sweptback wing (25-percent-chord line) of aspect ratio 3, taper ratio 0.2, and having an NACA 65A004 thickness distribution for the streamwise airfoil section was mounted on the body in such a way that the trailing edge of the wing (the only straight-line element of the wing) was in a plane parallel to and 0.50 inch below the body center line.

The side-view photographs in figure 2 indicate the warped wing contour. The ordinates of the mean-line surface were designed to give low drag at a Mach number of 1.46 and a wing lift coefficient of 0.3. The ordinates were determined by the method given in the appendix and are tabulated in table III. The loadings used in the design method and other contour diagrams are shown in figures 3, 4, and 5. The one straight-line wing element (typical for this type warp) was located at the wing trailing edge for convenience in checking model alignment but presumably could have been placed at any other wing-chord location without altering the overall aerodynamic characteristics of the wing. The angle of incidence of the wing with respect to the body was selected to give approximately zero lift when the angle of attack of the body and the horizontal tail deflection were zero.

The model was of metal construction with a solid steel wing. A sustainer rocket motor was carried inside the fuselage in addition to a telemeter with angle-of-attack, angle-of-sideslip, pressure and accelerometer instruments. The model was externally boosted by two Deacon rockets firing together.

TEST

Data were obtained during ascent of the model after separation from the booster. During flight of the model alone, a square-wave pulse was continuously generated by the horizontal tail which automatically flipped between stop settings each time the lift on the tail reversed direction.

The quantities measured by the telemeter system were normal and longitudinal accelerations, angles of attack and sideslip, horizontal tail

deflection, and total pressure. The velocity obtained from CW Doppler radar set (corrected for wind velocity) was used in conjunction with tracking radar and radiosonde data to calculate Mach number, Reynolds number, and dynamic pressure. Ground rollsonde equipment operating with the directional telemeter antenna signal from the model indicated that the level of model rolling velocity varied between approximately -5 and 0 radians per second throughout the flight of the model alone with the maximum rolling velocity occurring at the highest Mach numbers. The variation of the free-stream Reynolds number per foot length and dynamic pressure with Mach number is shown in figure 6(a). There was a coasting period before and after the period of flight with sustainer power on. The ranges of the maximum angles of attack and induced sideslip are shown in figure 6(b).

ACCURACY AND CORRECTIONS

Reference 7 indicates the accuracy that can be expected of a typical flow indicator working without the telemeter apparatus. An estimated possible inaccuracy of about $\pm 0.4^\circ$ in the telemeter angle of attack would cause a rotation of the drag polar such that a discrepancy in total drag coefficient of ± 0.002 or in drag due to lift of $\pm 9\frac{1}{2}$ percent at a nominal lift coefficient of 0.3 and Mach number of 1.46 would result. Further errors in aerodynamic coefficients can arise because of dynamic-pressure inaccuracies which are approximately twice as large as the error in Mach number. Mach number is estimated to be accurate to ± 1 percent. Thus all coefficients have a probable error of at least ± 2 percent.

To avoid error in the determination of the drag polars that might result from either external or internal misalignment of the longitudinal accelerometer instrument when subjected to normal acceleration, the angularity of the mounting base in the model was measured, and the instrument itself was calibrated while subjected to normal acceleration. The "feet" of the accelerometer were ground to reduce the response of the instrument to normal-force interaction. The residual internal instrument error due to normal acceleration and the external misalignment of the instrument mounting base were accounted for in the data reduction.

An additional source of inaccuracy in the final results may be caused by the induced sideslip and rolling motions. These motions were of greater magnitude at the higher test Mach numbers.

Measurements obtained from the flow indicator were corrected for position error and flight-path curvature. Position corrections were also made to measurements obtained from the normal and longitudinal accelerometers mounted near the center of gravity of the model.

The probable errors are estimated to be less than the following possible limits of accuracy:

C_D at $C_L = 0$	± 0.001
C_D at $C_L = 0.3$	± 0.003
C_N	± 0.01
α , deg	± 0.4
C_m	± 0.02
M	± 0.01

RESULTS AND DISCUSSION

Drag

Figures 7 and 8 show the drag results obtained. The maximum wing lift coefficient was generally somewhat less than the wing design lift coefficient of 0.3, particularly at the higher Mach numbers. Comparison with the flat wing model of reference 6 shows approximately the same drag for the two models at the highest test lift coefficients. At zero lift coefficient the wing twist and camber increased the drag coefficient by the amount 0.002 or 5 percent at the design Mach number of 1.46 and 0.003 or 10 percent at a Mach number of 2.1. Figure 8 further shows that by comparison with the body-tail model (ref. 8) at zero lift this increase in drag due to wing warp corresponds to a 20-percent increase in the drag coefficient of a wing with interference at a Mach number of 1.46 and a 50-percent increase at a Mach number of 2.1.

The drag results of this test and the swept-wing model test of reference 2 indicate that for a swept wing a lift coefficient of 0.3 does not give a reduction in drag due to lift at the supersonic Mach numbers tested and at lift coefficients up to 0.6. However, the tests of references 2 and 3 do show drag reductions for delta and swept wings designed for a lift coefficient of approximately 0.2. Figure 14 of reference 2 shows that for the swept wing of that test there is an optimum value of the design lift coefficient slightly below a value of 0.2. This is a result not predicted by the theory. If this result of reference 2 had been available when the model wing of the present test was designed, a lower design lift coefficient would have been selected.

Total Normal Force and Pitching Moment

Figure 9 to 11 present plots of normal-force and pitching-moment coefficients and summarize the variation of the normal-force-curve and

~~CONFIDENTIAL~~

pitching-moment-curve slopes with Mach number. Figure 9 shows that the variation of normal-force coefficient with angle of attack is linear within the range tested. The variation of pitching-moment coefficient with normal-force coefficient presented in figure 10 is approximately linear for positive values of normal-force coefficient and slightly nonlinear for negative values. The variation with Mach number of normal-force-curve slope $C_{N\alpha}$ and static stability parameter $\frac{dC_m}{dC_N}$ presented in figure 11 parallels the corresponding result for the flat wing model of reference 6. The wing twist and camber increased $C_{N\alpha}$ approximately 0.004 and increased the static margin approximately 0.05c.

Wash at the Horizontal Tail

Effective wash at the horizontal tail was determined at the start of each tail flip when the lift on the tail was assumed to be zero and the air flow parallel to the tail chord plane. The following equation was used to evaluate the wash:

$$\text{Wash} \approx -\alpha_{\text{flip}} - \delta$$

Figure 12 shows that at positive angles of attack and the negative tail setting, the value of α_{flip} was about 1.2° . For negative angles of attack and the positive tail setting, the α_{flip} was about -0.3° .

This indicates less upwash at the tail for the positive values of α_{flip} and more for the negative values. This asymmetry is believed to be due to the influence of the inboard region of the wing which had a positive incidence to the fuselage of the order of 1.6° .

CONCLUDING REMARKS

An investigation of the effect of wing camber and twist on the supersonic lift, drag, and stability characteristics of a rocket-powered model having a 52.5° swept wing of aspect ratio 3 and inline tail surfaces leads to the following observations:

1. Although the maximum wing loading was generally less than that required for a wing design lift coefficient of 0.3, the twisted- and cambered-wing model had approximately the same drag coefficient as the flat wing model at the highest test lift coefficients and at the same Mach number.

2. The wing twist and camber increased the minimum drag coefficient by the amounts 0.002 at the wing design Mach number of 1.46 and 0.003 at a Mach number of 2.1.

3. The wing warp also increased the normal-force-curve slope approximately 0.004 and the static margin approximately 0.05c.

Langley Aeronautical Laboratory,
National Advisory Committee for Aeronautics,
Langley Field, Va., February 27, 1956.

APPENDIX

DESIGN PROCEDURE USED FOR TWISTED AND CAMBERED WING

The design procedure used to determine the wing twist and camber required for low wing drag at a design Mach number of 1.46 and a wing lift coefficient of 0.3 was based on the wing-warping method of reference 4 and was similar to the procedure outlined in the appendix of reference 3.

The assumed variation of the lifting pressure coefficient described by equation (2) of reference 4 was used to obtain the load distribution:

$$\frac{P}{C_L} = \frac{C_1}{C_L} + \frac{1-k}{1-\lambda} \frac{C_2}{C_L} \frac{x}{c_r} + \frac{C_3}{C_L}(\sigma) + \frac{C_4}{C_L}(\sigma)^2$$

The values of the constants $\frac{C_1}{C_L}$, $\frac{C_2}{C_L}$, and $\frac{C_4}{C_L}$ were expressed in terms of $\frac{C_3}{C_L}$ (eqs. 22, 23, and 24 of ref. 4):

$$\frac{C_1}{C_L} = \frac{4k(1+\lambda)}{(1+k)\pi} + \frac{1-k}{(1-\lambda)(1+k)} \frac{C_3}{C_L}$$

$$\frac{C_2}{C_L} = \frac{4(1-\lambda^2)}{(1+k)\pi} - \frac{2}{(1+k)} \frac{C_3}{C_L}$$

$$\frac{C_4}{C_L} = \frac{6(1+\lambda)}{(1+3\lambda) - 6(1+\lambda)A} \left[1 - \frac{8(1+\lambda) - 4\lambda^2}{3\pi} + \frac{(4-2\lambda)(1+\lambda)}{\pi} A \right]$$

where $A \equiv \frac{\lambda^2(1-k)}{(k+n)(1-\lambda^2)}$ and $n = m\sqrt{M^2 - 1}$. A value of $n = 0.7$ was selected with a corresponding design Mach number of 1.46. The value of $\frac{C_3}{C_L}$ was determined from a condition imposed on the chordwise load distribution. This condition was that the slope of the chordwise loading at $x/c_r = 1.0$ be zero. The chordwise loading in the region $0 \leq \frac{x}{c_r} \leq 1.0$ is given by:

$$\frac{b'c_l'}{bC_L} = \frac{C_1}{C_L} a \frac{x}{c_r} + \left(\frac{C_2}{C_L} + \frac{C_3}{2C_L} \right) a^2 \left(\frac{x}{c_r} \right)^2 + \frac{C_4}{3C_L} a^3 \left(\frac{x}{c_r} \right)^3$$

where $a \equiv \frac{2c_r}{b}$ and $m \equiv \frac{1-k}{1-\lambda} = 0.728$. The final numerical values of the four constants were as follows:

$$\frac{C_1}{C_L} = 1.582$$

$$\frac{C_2}{C_L} = -2.241$$

$$\frac{C_3}{C_L} = 2.200$$

$$\frac{C_4}{C_L} = 0.149$$

The chordwise and spanwise loadings corresponding to this set of constants are shown in figure 4. For comparative purposes, elliptic loadings are also shown in the figure. The drag due to lift of the resulting warped wing was calculated by a method of graphical integration and found to be approximately the same as for the flat wing with full leading-edge suction. This result prompted the present test.

REFERENCES

1. Hall, Charles F.: Lift, Drag, and Pitching Moment of Low-Aspect-Ratio Wings at Subsonic and Supersonic Speeds. NACA RM A53A30, 1953.
2. Boyd, John W., Migotsky, Eugene, and Wetzell, Benton E.: A Study of Conical Camber for Triangular and Sweptback Wings. NACA RM A55G19, 1955.
3. Burrows, Dale L., and Tucker, Warren A.: A Transonic Wind-Tunnel Investigation of the Static Longitudinal Characteristics of a 3-Percent-Thick, Aspect-Ratio-3, Delta Wing Cambered and Twisted for High Lift-Drag Ratios. NACA RM L55F02a, 1955.
4. Tucker, Warren A.: A Method for the Design of Sweptback Wings Warped to Produce Specified Flight Characteristics at Supersonic Speeds. NACA Rep. 1226, 1955. (Supersedes NACA RM L51F08.)
5. Grant, Frederick C.: The Proper Combination of Lift Loadings for Least Drag on a Supersonic Wing. NACA TN 3533, 1955.
6. Gillespie, Warren, Jr.: Lift, Drag, and Longitudinal Stability at Mach Numbers From 1.4 to 2.3 of a Rocket-Powered Model Having a 52.5° Sweptback Wing of Aspect Ratio 3 and Inline Tail Surfaces. NACA RM L55I12, 1955.
7. Ikard, Wallace L.: An Air-Flow-Direction Pickup Suitable for Telemetering Use on Pilotless Aircraft. NACA RM L53K16, 1954.
8. Gillespie, Warren, Jr., and Dietz, Albert E.: Rocket-Powered Model Investigation of Lift, Drag, and Stability of a Body-Tail Configuration at Mach Numbers From 0.8 to 2.3 and Angles of Attack Between $\pm 6.5^\circ$. NACA RM L54C04, 1954.

TABLE I.- CONTOUR ORDINATES OF NOSE

Station, in. from nose	Body radius, in.
0	0.17
.06	.18
.12	.21
.24	.22
.48	.28
.73	.35
1.22	.46
2.00	.64
2.45	.73
4.80	1.24
7.35	1.72
8.00	1.85
9.80	2.15
12.25	2.50
13.12	2.61
14.37	2.75
14.70	2.78
17.15	3.01
19.60	3.22
22.05	3.38
24.50	3.50
25.00	3.50

TABLE II.- CHARACTERISTICS OF MODELS

Wing:

Span, ft	3.46
Area, sq ft	4.0
Aspect ratio	3.0
Taper ratio	0.2
Sweepback of 0.25 chord, deg	52.5
Mean aerodynamic chord, \bar{c} , ft	1.32
Airfoil-section thickness distribution	
about mean camber line, streamwise.	NACA 65A004
Incidence at 0.2 half span, deg	1.6

Body:

Maximum diameter, ft	0.58
Base diameter, ft	0.42
Length, ft	9.85
Fineness ratio	16.9
Boat-tail angle, deg	2.16

Horizontal tail:

Span, ft	1.85
Aspect ratio	2.7
Sweepback of 0.50 chord, deg	0
Airfoil section	4 percent hexagonal

Vertical tail:

Span, ft	1.67
Aspect ratio	1.08
Sweepback of leading edge, deg	70
Sweepback of trailing edge, deg	15
Airfoil section	1/4-inch beveled flat plate

Model weight, lb:

With sustainer rocket loaded	195
With sustainer rocket empty	150

Moment of inertia in pitch, slug-ft²:

With sustainer rocket loaded	27.6
With sustainer rocket empty	24.7

Center of gravity with sustainer rocket:

loaded or empty, percent \bar{c} behind leading edge	
of mean aerodynamic chord	55

TABLE III. - WING ORDINATES MEASURED FROM WING APEX AND FROM A
REFERENCE PLANE 1.500 INCHES BELOW MODEL CENTER LINE

At 4.16 in. outboard			At 8.31 in. outboard			At 12.47 in. outboard			At 16.63 in. outboard			At 20.78 in. outboard																										
X (a)	Y _L (b)	Y _U (b)	X (a)	Y _L (b)	Y _U (b)	X (a)	Y _L (b)	Y _U (b)	X (a)	Y _L (b)	Y _U (b)	X (a)	Y _L (b)	Y _U (b)																								
6.35	1.548	1.548	12.70	0.965	0.965	19.05	0.707	0.707	25.40	0.589	0.589	31.75	0.524	0.524																								
6.50	1.509	1.640	12.75	.940	1.005	19.25	.685	.804	25.50	.575	.638	31.875	.525	.581																								
6.75	1.485	1.713	13.00	.926	1.106	19.375	.685	.845	25.625	.575	.690	32.00	.533	.620																								
7.00	1.475	1.765	13.25	.932	1.168	19.50	.688	.880	25.75	.585	.720	32.125	.548	.655																								
7.25	1.470	1.806	13.50	.940	1.215	19.625	.695	.910	25.875	.590	.732	32.25	.563	.686																								
7.50	1.465	1.840	13.75	.943	1.257	19.75	.705	.950	26.00	.606	.780	32.375	.579	.712																								
7.75	1.458	1.865	14.00	.945	1.293	20.00	.715	.979	26.125	.615	.802	32.50	.594	.740																								
8.00	1.451	1.890	14.25	.945	1.324	20.25	.731	1.002	26.25	.625	.826	32.75	.625	.786																								
8.50	1.436	1.930	14.50	.946	1.352	20.50	.741	1.055	26.50	.640	.863	33.00	.653	.825																								
9.00	1.412	1.955	15.00	.948	1.400	20.75	.749	1.090	27.00	.660	.931	33.25	.680	.859																								
9.50	1.390	1.980	15.50	.945	1.440	21.00	.758	1.115	27.50	.685	.985	33.50	.702	.890																								
10.00	1.365	1.995	16.00	.942	1.465	22.00	.773	1.200	28.00	.707	1.024	34.00	.750	.935																								
11.00	1.315	2.004	17.00	.953	1.504	23.00	.785	1.245	28.50	.730	1.058	34.50	.780	.960																								
12.00	1.255	1.991	18.00	.960	1.557	24.00	.794	1.271	29.00	.754	1.084	35.00	.822	.985																								
13.00	1.206	1.960	19.00	.915	1.590	25.00	.810	1.280	29.50	.779	1.100	35.50	.905	.995																								
14.00	1.150	1.925	20.00	.907	1.551	26.00	.856	1.262	30.00	.802	1.109	36.00	.957	1.000																								
15.00	1.105	1.881	21.00	.905	1.502	27.00	.862	1.235	30.50	.832	1.114	36.57	1.000	1.000																								
16.00	1.065	1.825	22.00	.905	1.460	28.00	.895	1.185	31.00	.857	1.110	Leading-edge radius, 0.0047 Trailing-edge radius, 0.00046 Chord length, 4.62																										
17.00	1.040	1.757	23.00	.910	1.405	29.00	.926	1.150	31.50	.887	1.100																											
18.00	1.015	1.682	24.00	.923	1.340	30.00	.958	1.065	32.00	.913	1.086																											
19.00	.993	1.598	25.00	.939	1.270	31.00	.995	1.005	33.00	.965	1.041																											
20.00	.975	1.508	26.00	.953	1.195	31.062	1.000	1.000	33.72	1.000	1.000	Leading-edge radius, 0.009 Trailing-edge radius, 0.0003 Chord length, 8.52																										
21.00	.957	1.415	27.00	.970	1.110	Leading-edge radius, 0.012 Trailing-edge radius, 0.001 Chord length, 12.012			Leading-edge radius, 0.009 Trailing-edge radius, 0.0003 Chord length, 8.52																													
22.00	.935	1.325	28.00	.991	1.031																																	
23.00	.960	1.225	28.41	1.000	1.000																																	
24.00	.977	1.135	Leading-edge radius, 0.016 Trailing-edge radius, 0.002 Chord length, 15.71																																			
25.00	.990	1.055																																				
25.754	1.000	1.000																																				
Leading-edge radius, 0.020 Trailing-edge radius, 0.002 Chord length, 19.404																																						

^aMeasured from wing apex.

^bMeasured from a reference plane.

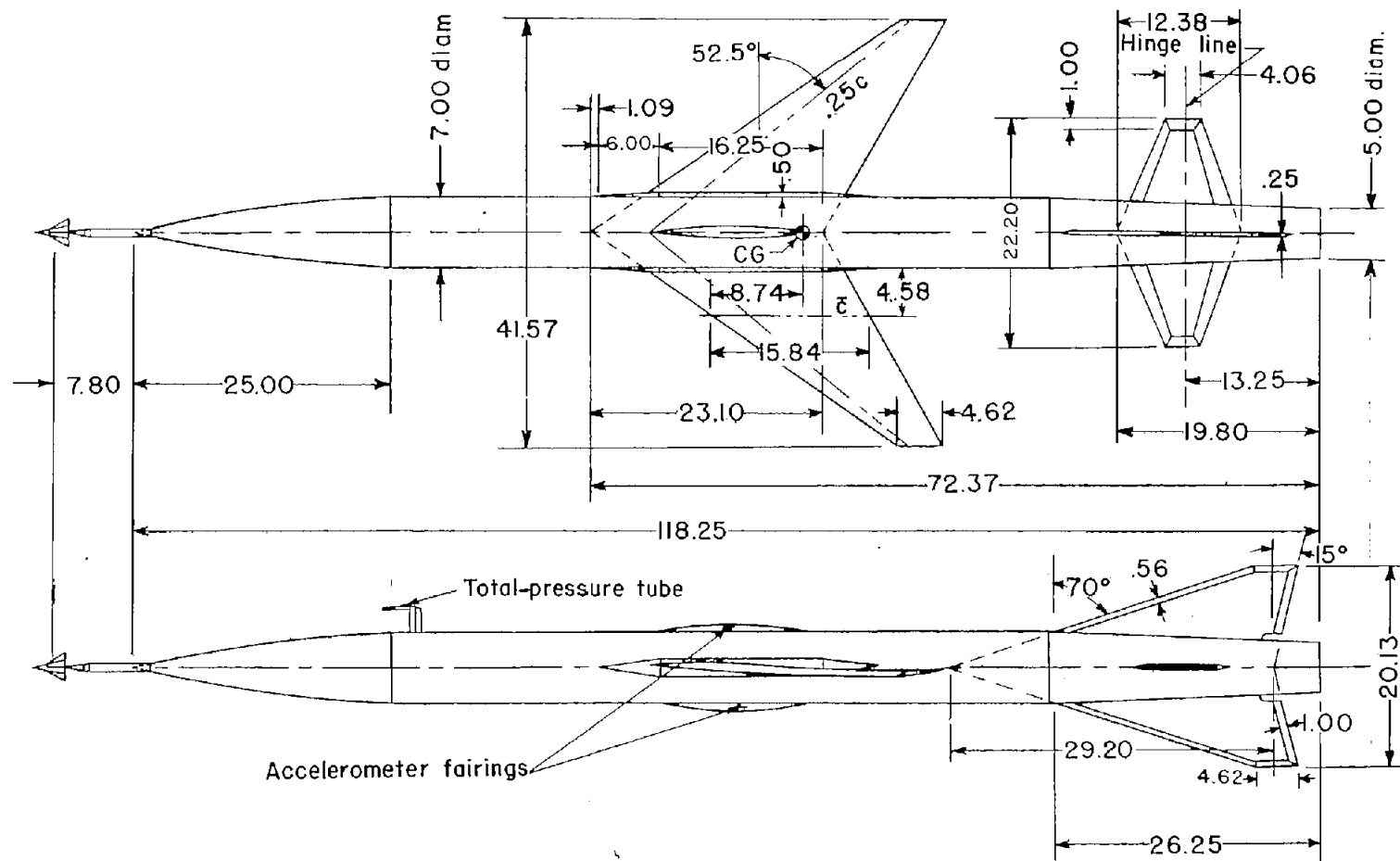
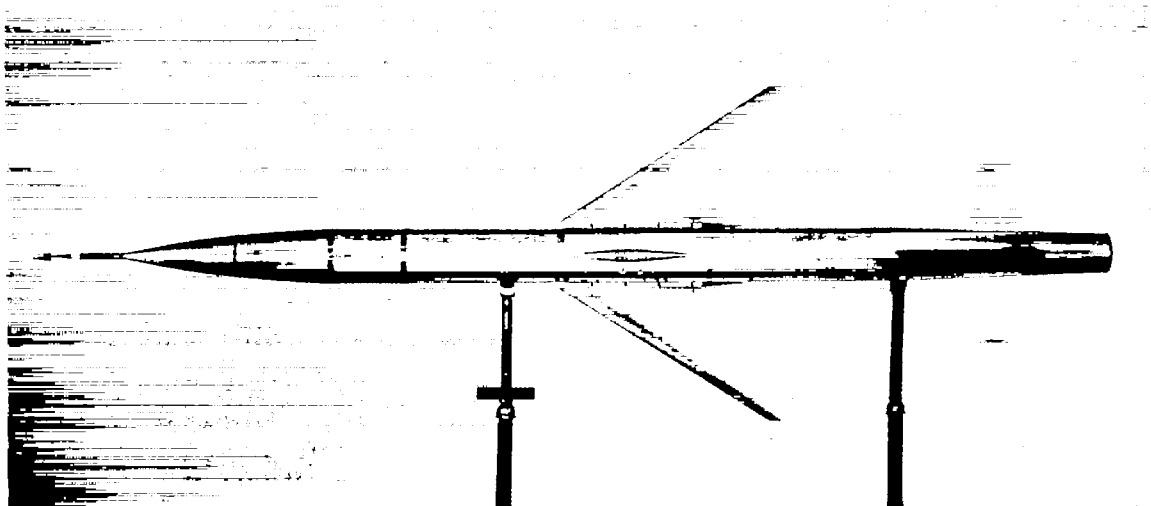
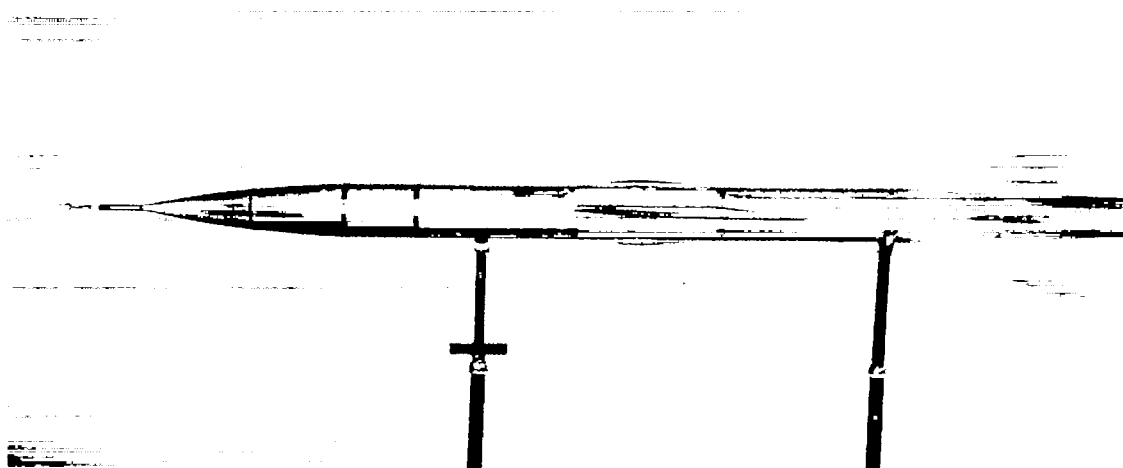


Figure 1.- Test configuration. All linear dimensions are in inches.



(a) Plan view.

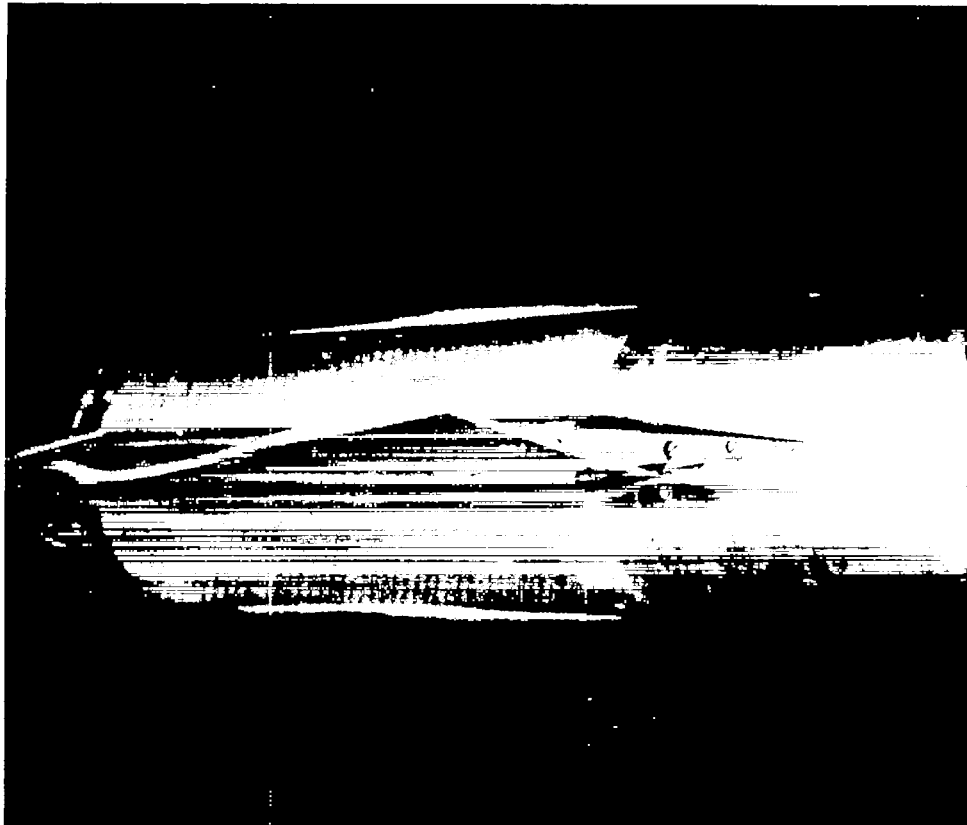
L-87463.1



(b) Side view.

L-87462.1

Figure 2.- Photographs of model with twisted and cambered wing.



(c) Closeup showing twisted and cambered wing. L-87461

Figure 2.- Concluded.

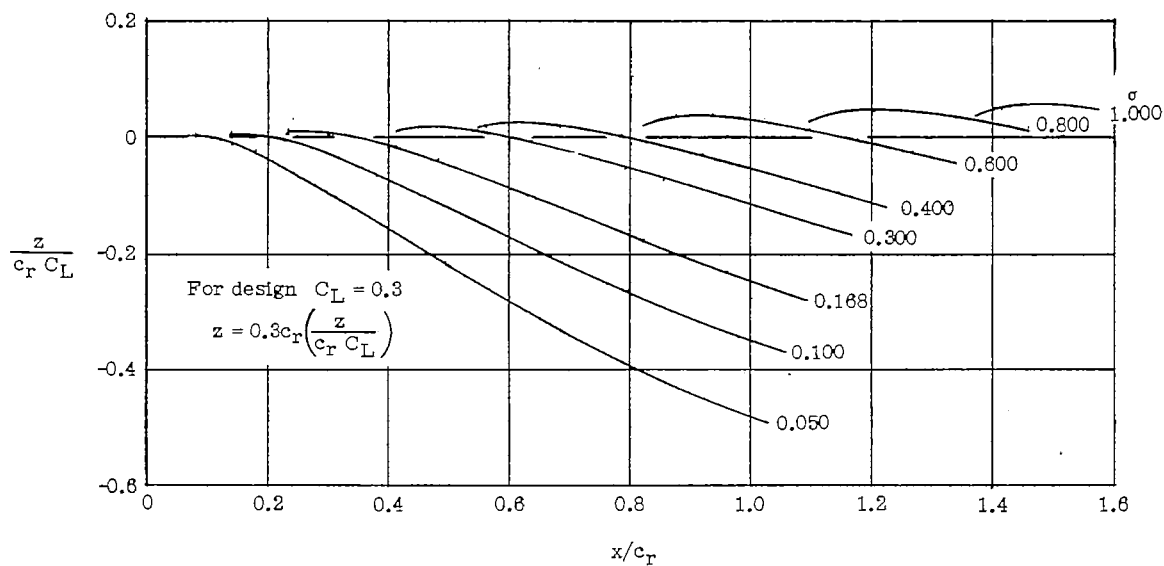
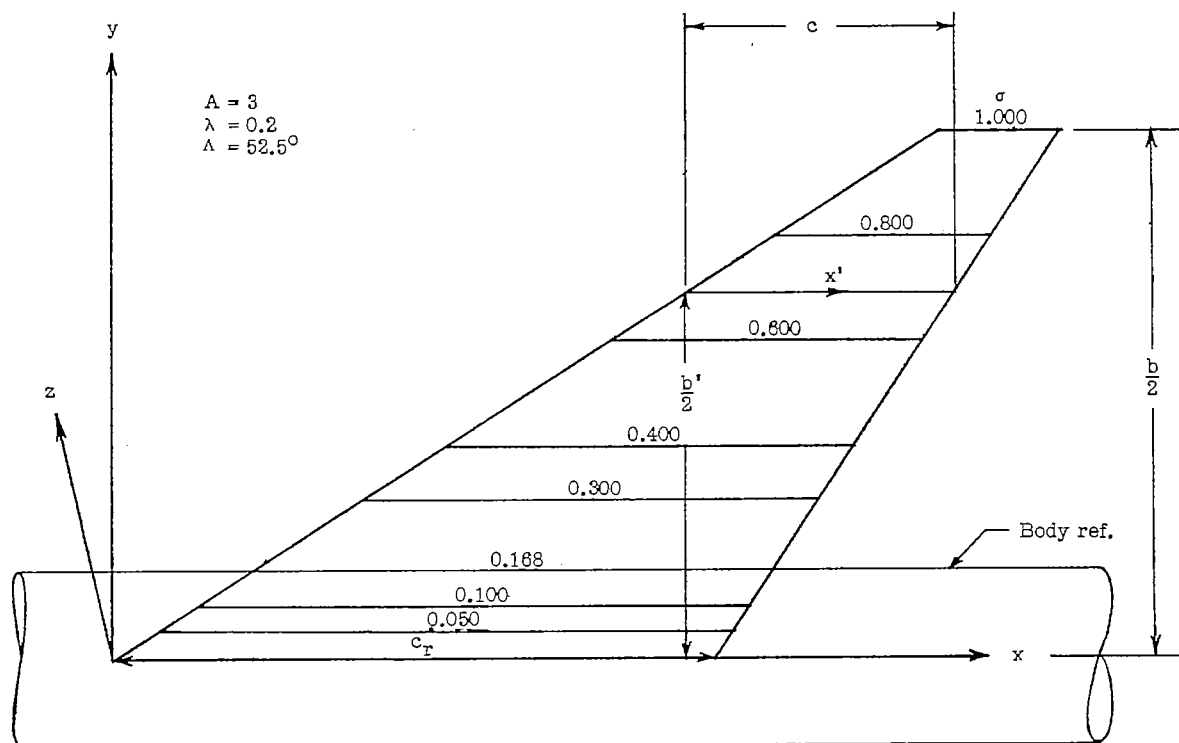


Figure 3.- Calculated wing warp for Mach number 1.46.

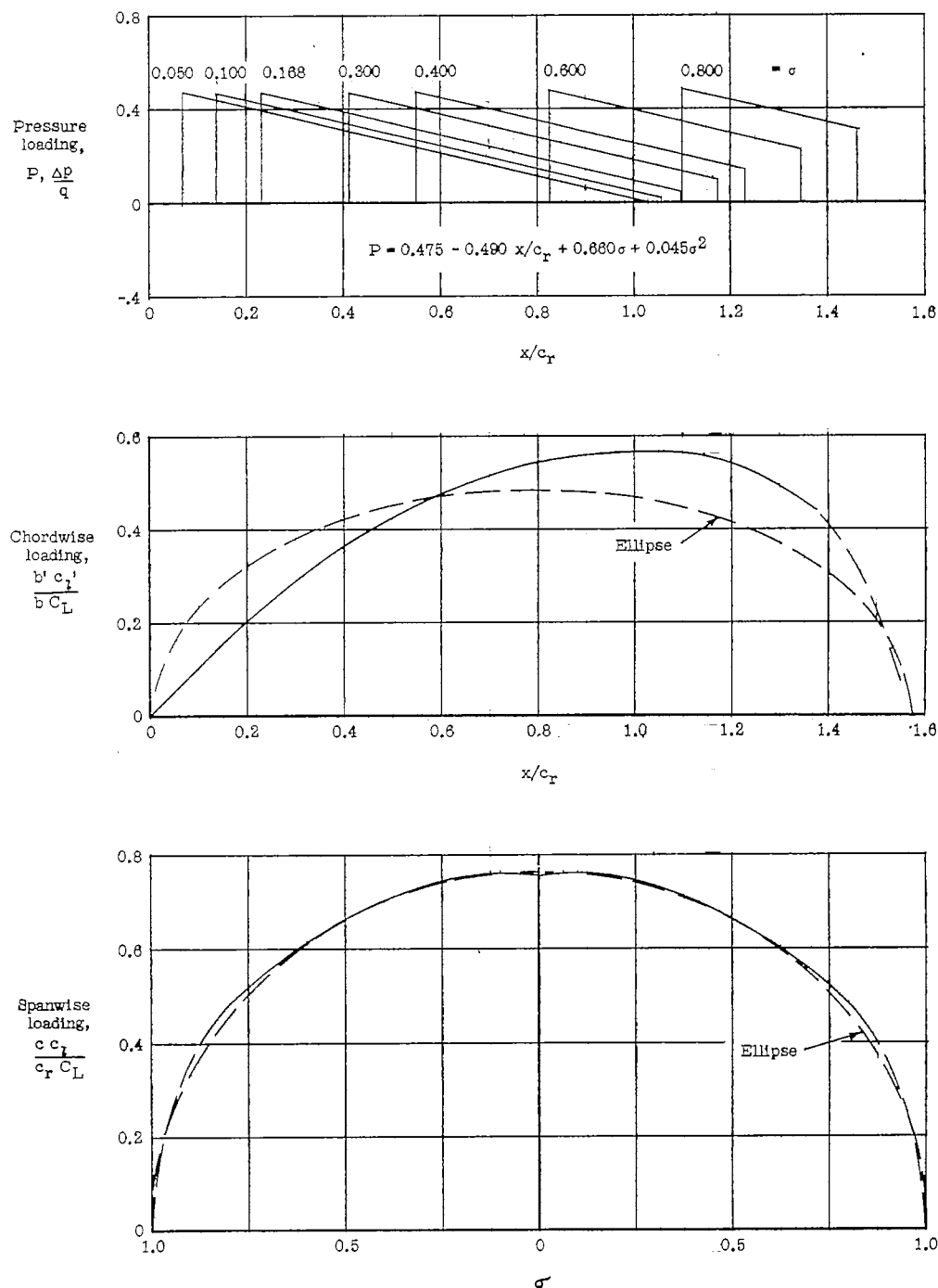


Figure 4.- Calculated pressure and load distributions for warped wing at $M = 1.46$ and $C_L = 0.3$.

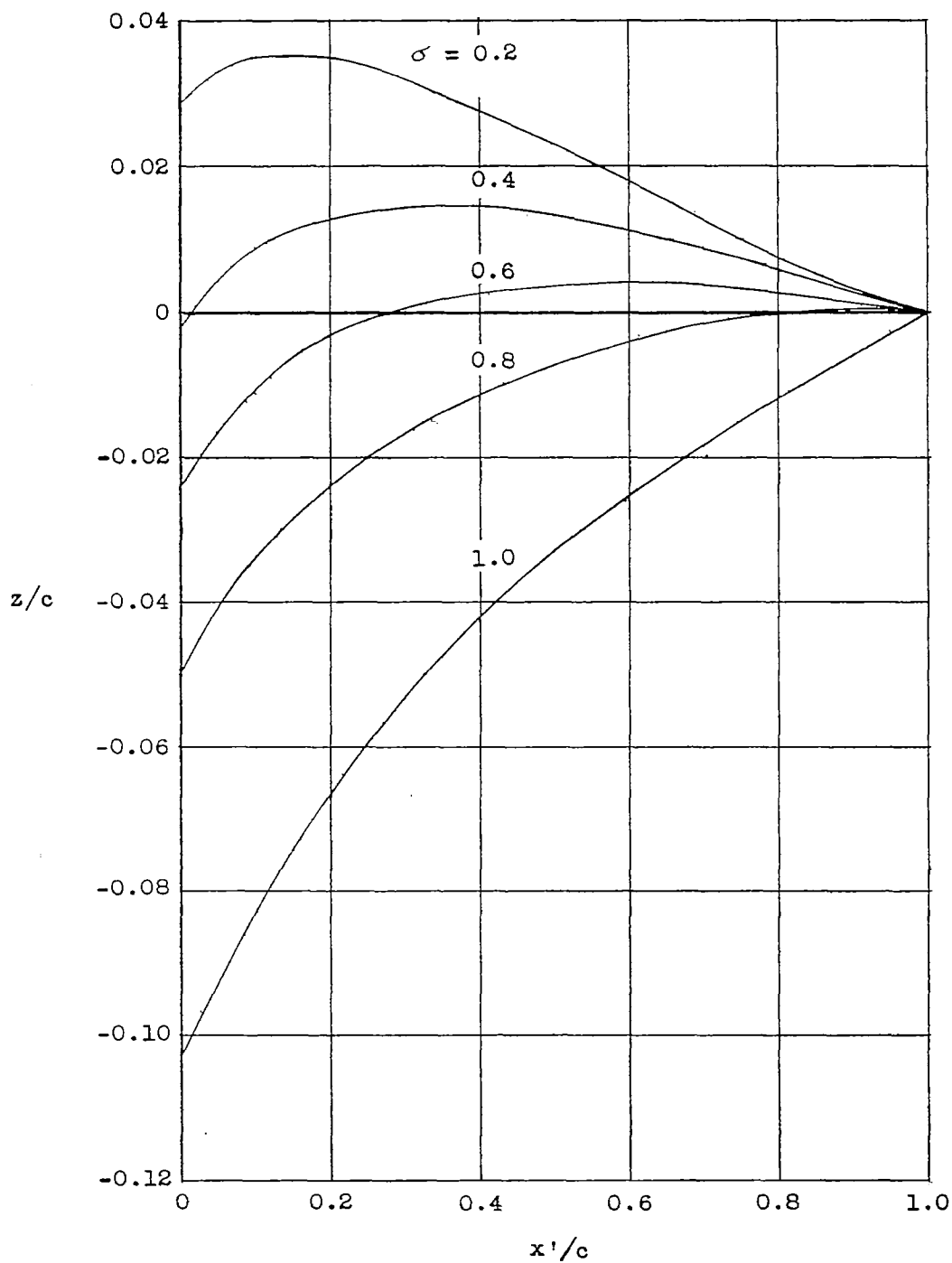
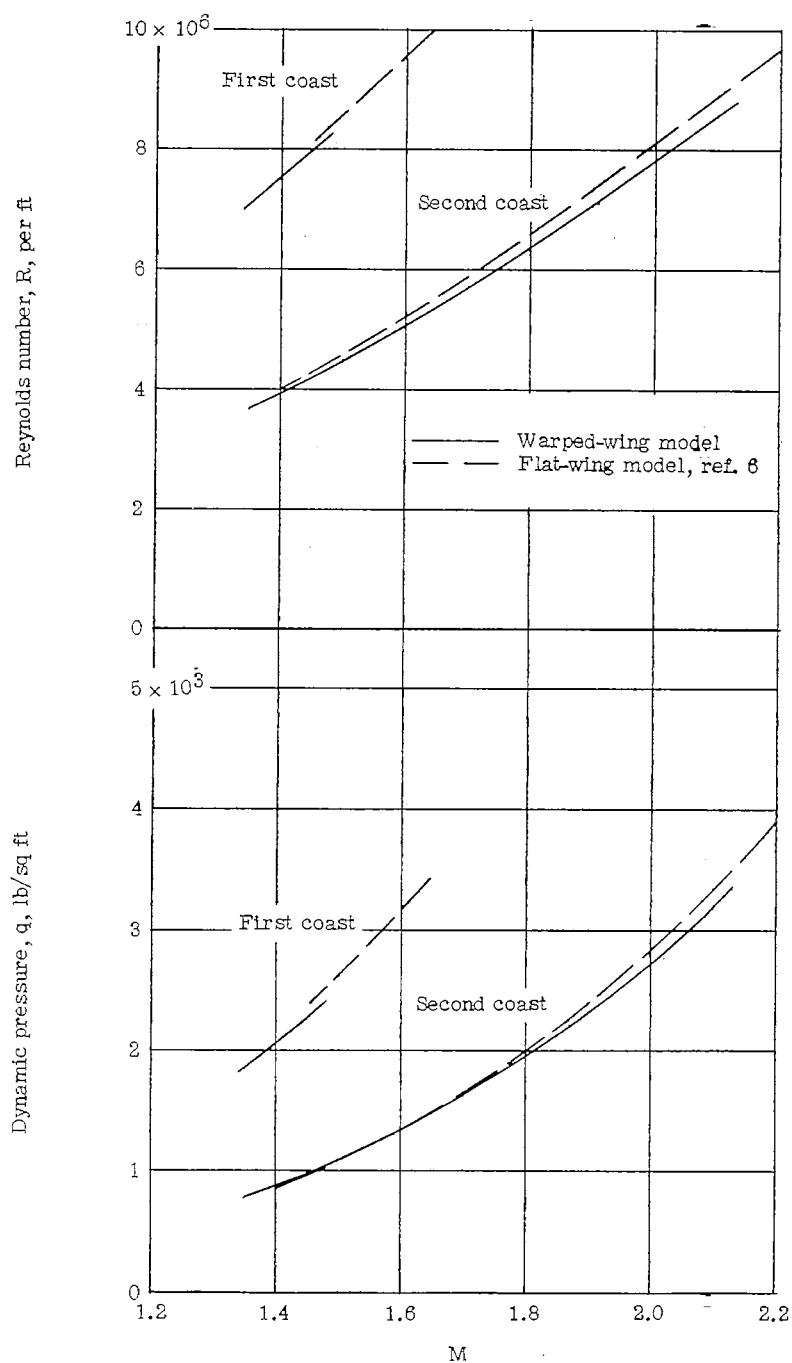
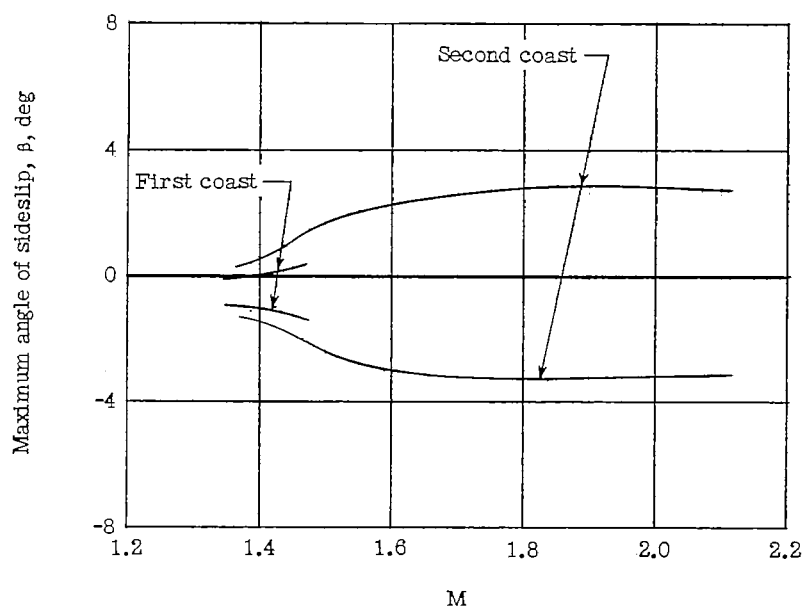
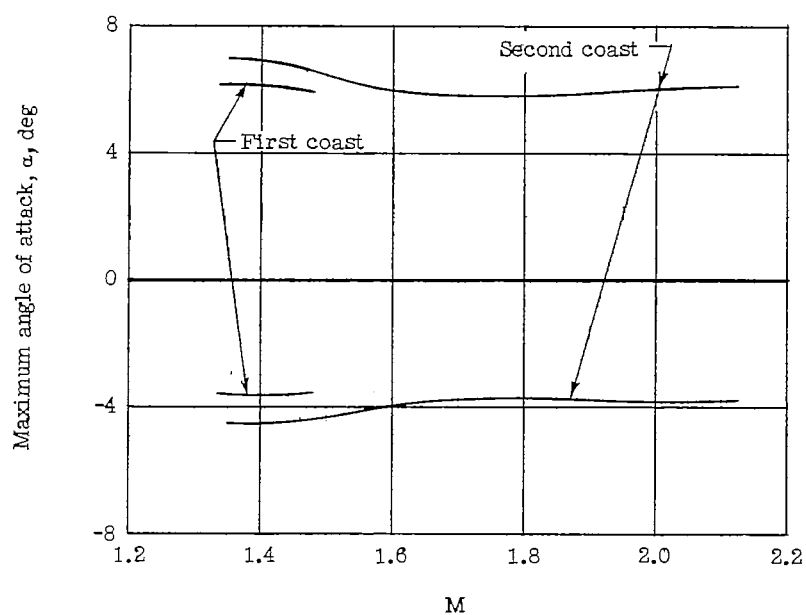


Figure 5.- Mean-line ordinates of warped wing in terms of the local chord with wing incidence of 1.6° at 0.2 half span.



(a) Reynolds number and dynamic pressure.

Figure 6.- Flight test conditions.



(b) Maximum angle of attack and induced sideslip.

Figure 6.- Concluded.

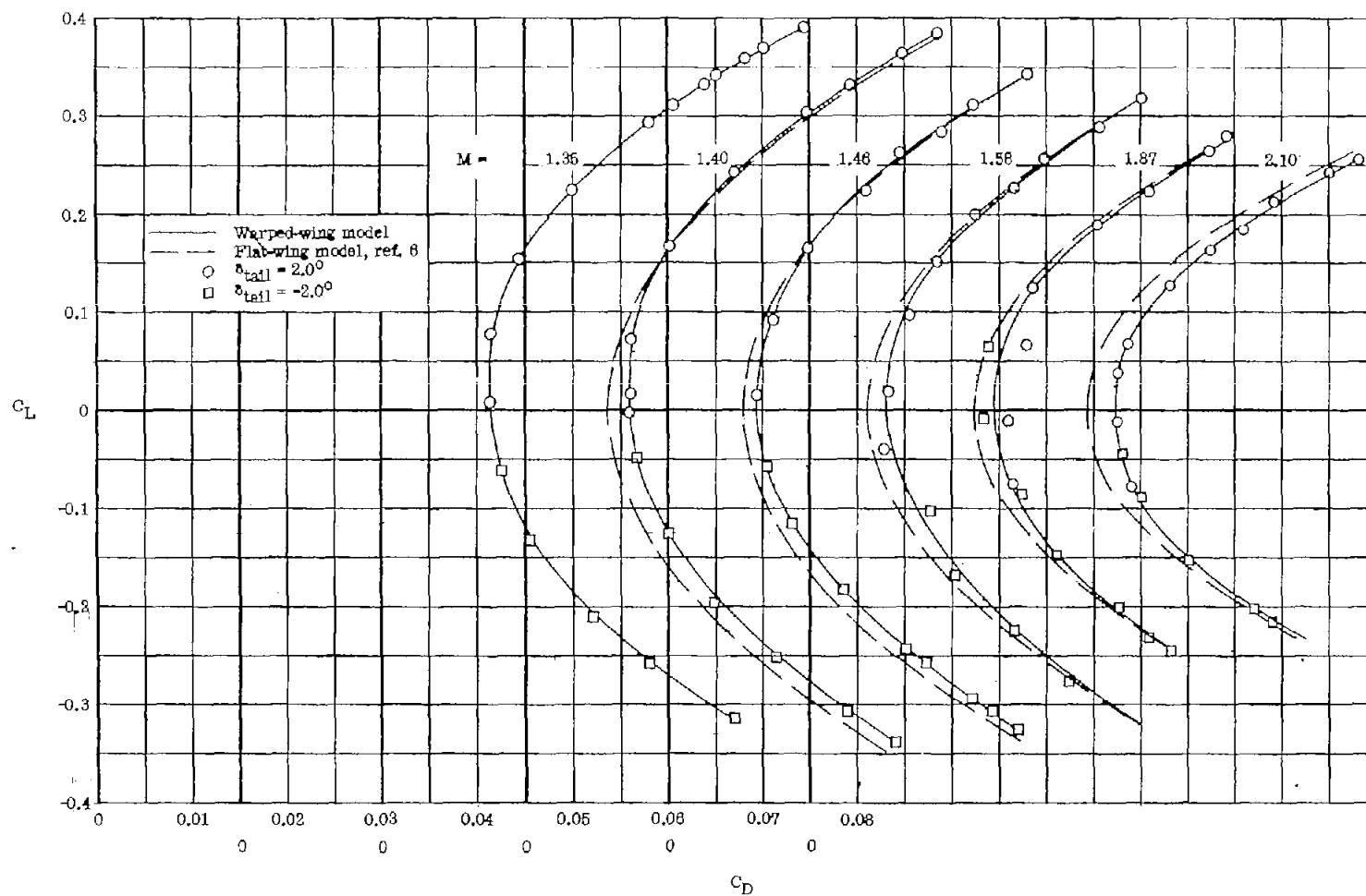


Figure 7.- Drag polars.

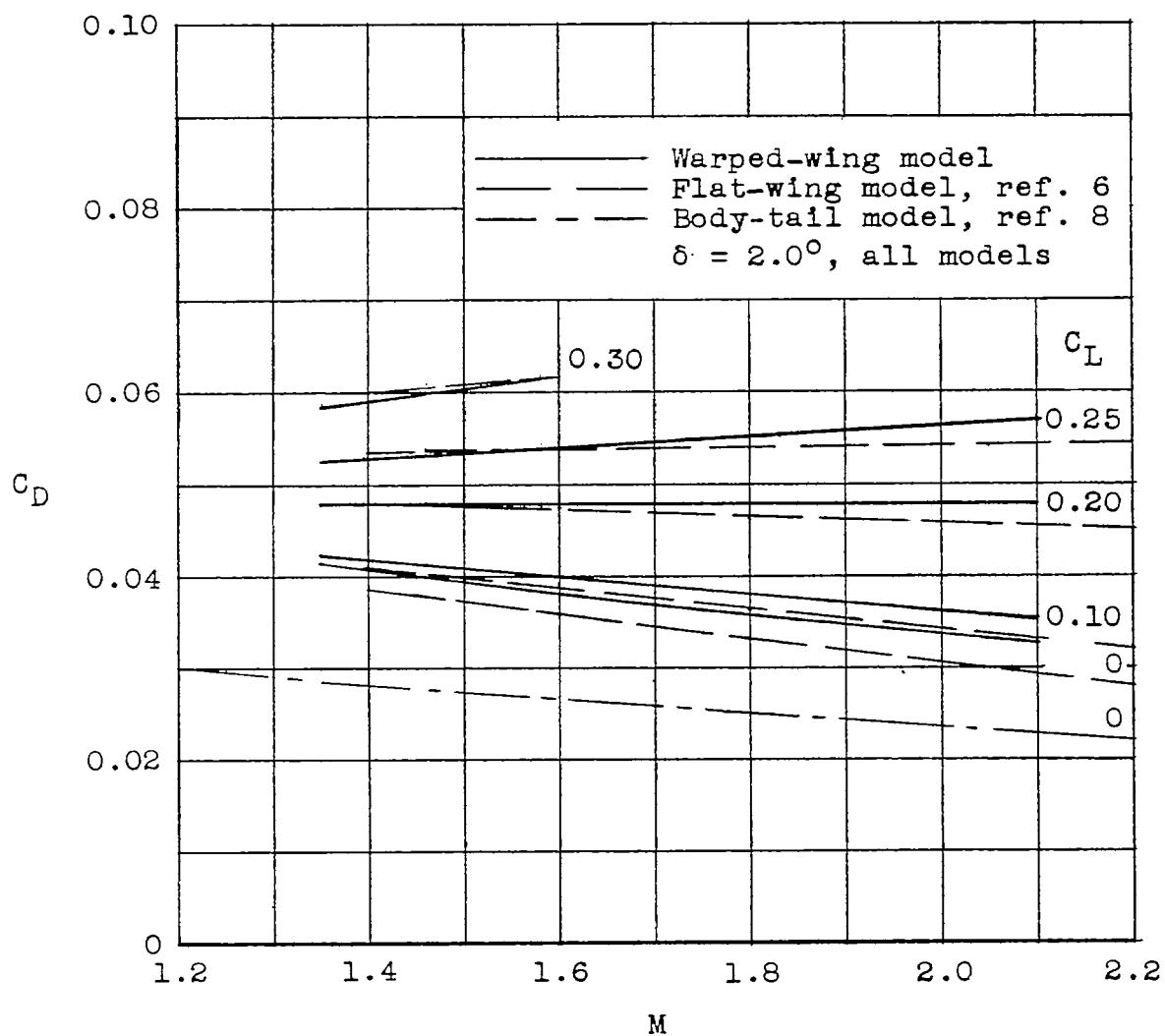
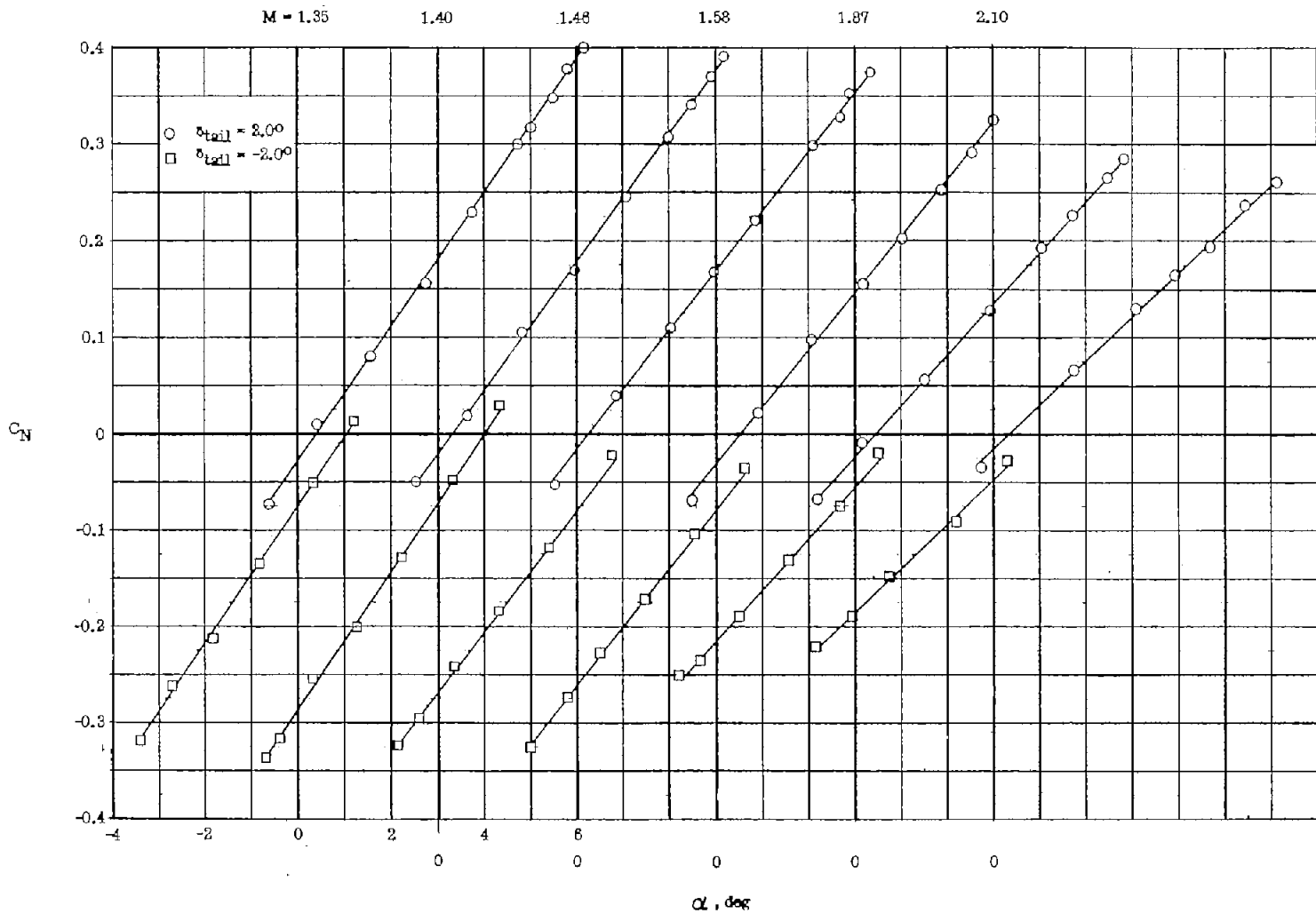


Figure 8.- Variation of drag coefficient with Mach number at various values of lift coefficient.

Figure 9.- Normal-force coefficient against α .

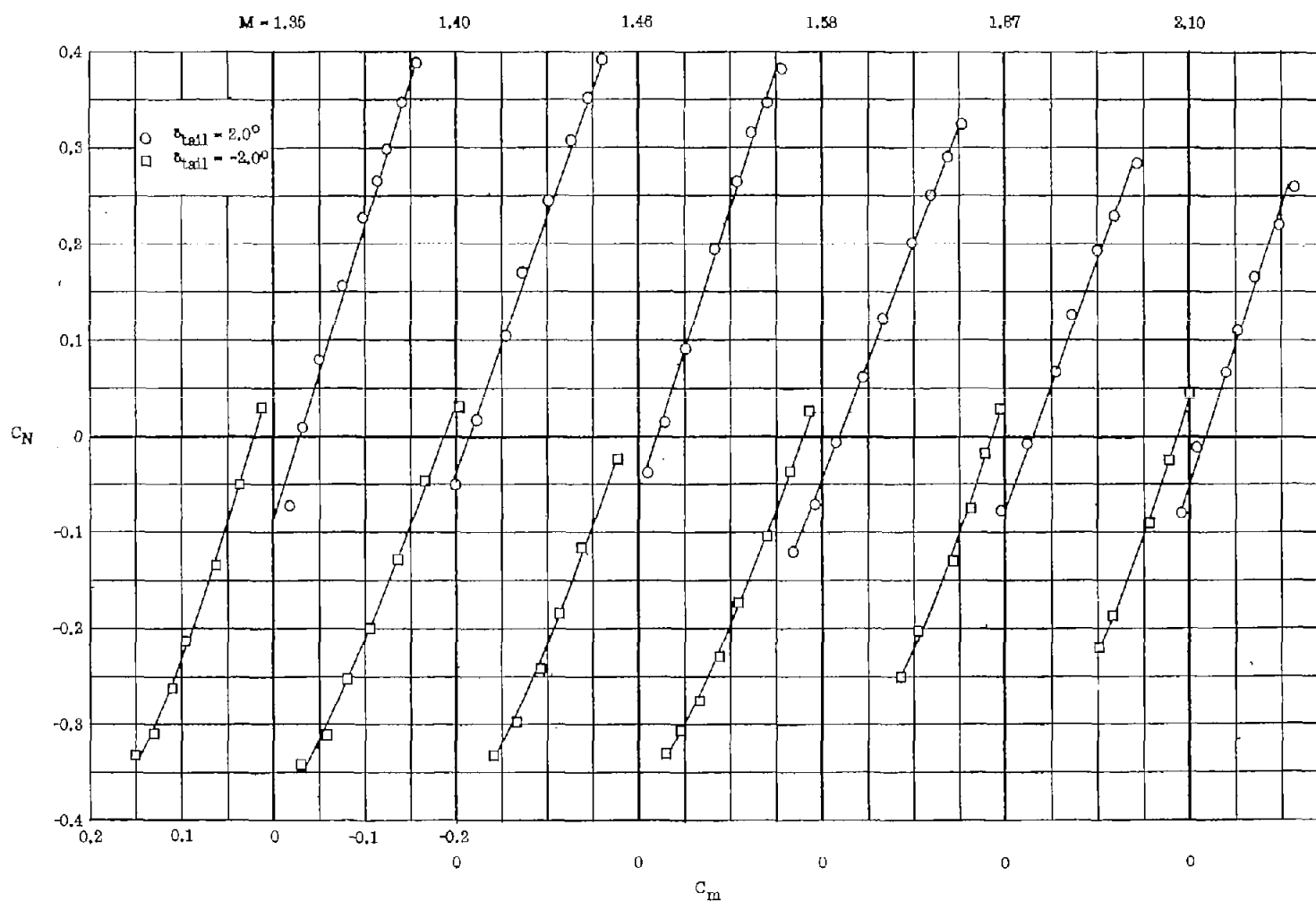


Figure 10.- Normal-force coefficient against pitching-moment coefficient.
Model center of gravity at 0.55 mean aerodynamic chord \bar{c} .

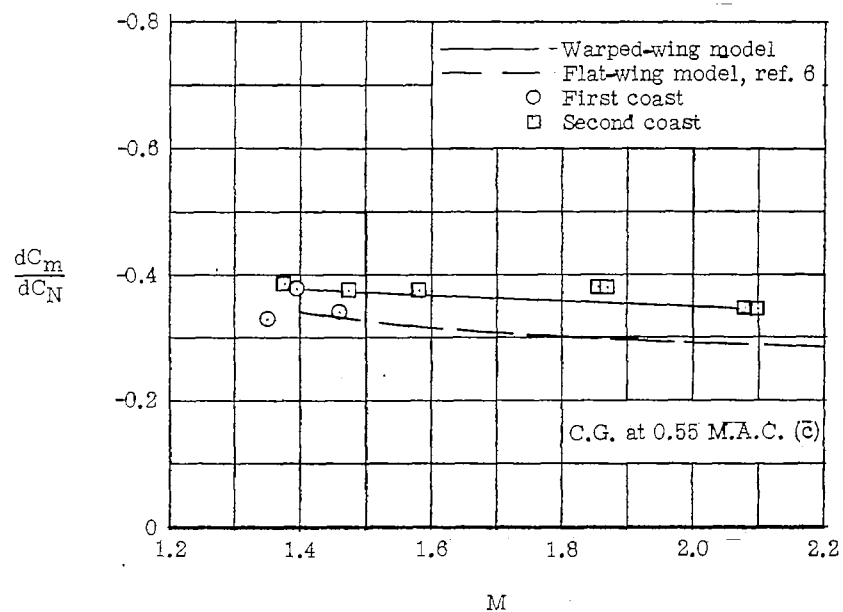
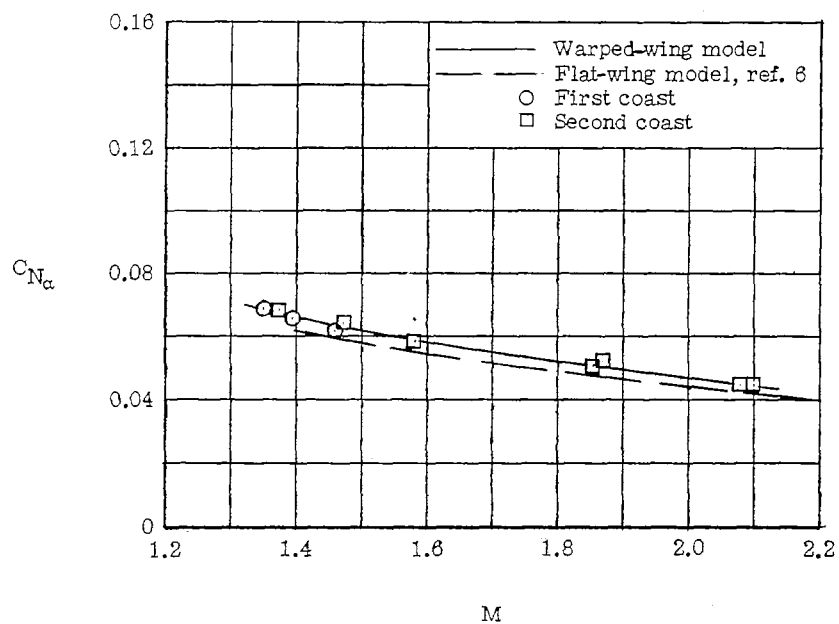
~~CONFIDENTIAL~~

Figure 11.- Variation of $C_{N\alpha}$ and dC_m/dC_N with Mach number.

~~CONFIDENTIAL~~

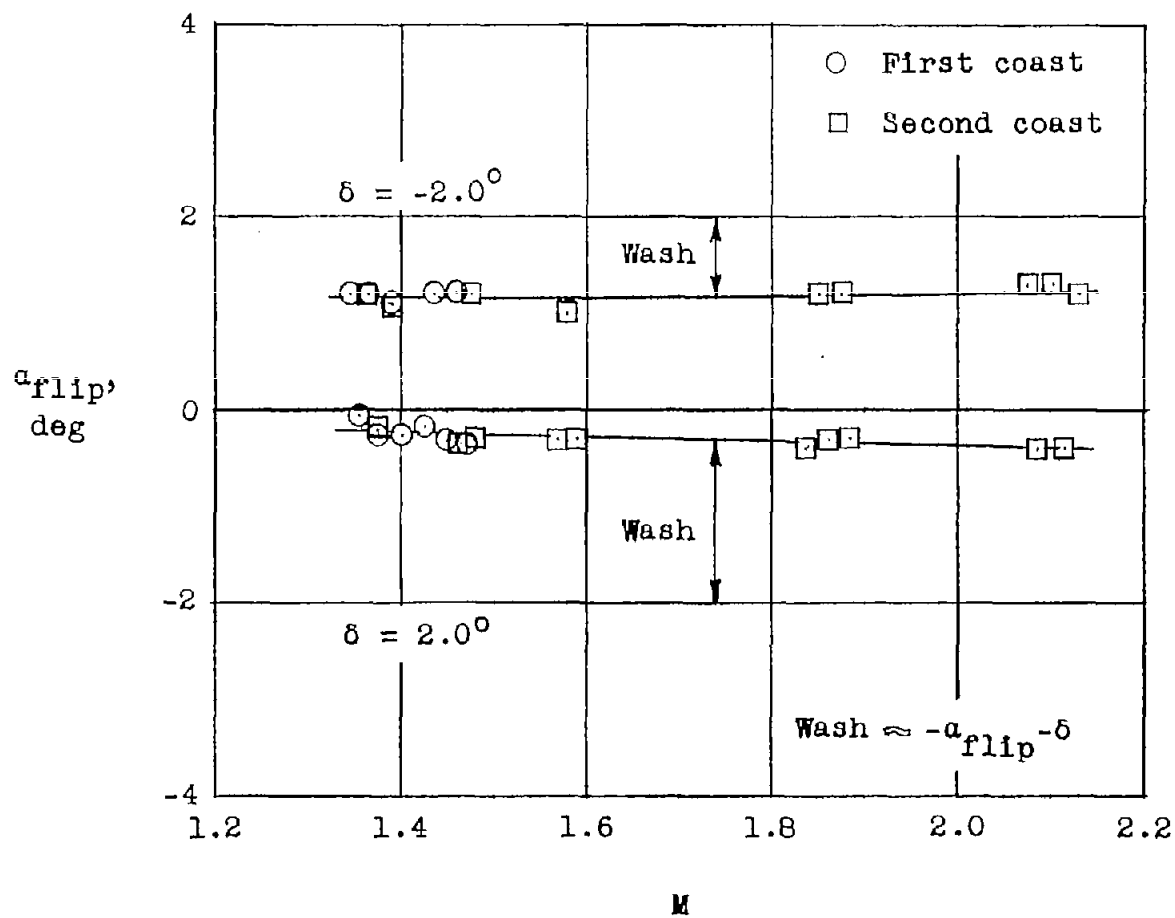


Figure 12.- Wash indicated by start of tail flip.